JACS
JOURNAL OF THE AMERICAN CHEMICAL SOCIETY
Article
pubs.acs.org/JACS

Toward the Synthesis of Sub-15 nm Ag Nanocubes with Sharp Corners and Edges: The Roles of Heterogeneous Nucleation and Surface Capping

Aleksey Ruditskiy[†] and Younan Xia*[,†,‡,§]

[†]School of Chemistry and Biochemistry, Georgia Institute of Technology, Atlanta, Georgia 30332, United States
[‡]The Wallace H. Coulter Department of Biomedical Engineering, Georgia Institute of Technology and Emory University, Atlanta, Georgia 30332, United States
[§]School of Chemical and Biomolecular Engineering, Georgia Institute of Technology, Atlanta, Georgia 30332, United States

Supporting Information

ABSTRACT: We report a polyol method for the facile synthesis of Ag nanocubes having sharp corners and edges, together with edge lengths below 15 nm. The rapid nucleation of Ag atoms was facilitated through the addition of a trace amount of SH^- to generate Ag_2S clusters while the corners and edges of the nanocubes were sharpened through the introduction of Br^- as a regulator of the growth kinetics and a capping agent for the Ag(100) surface. Because of their much smaller size relative to the more commonly used capping agent based on poly(vinylpyrrolidone), Br^- ions are more effective in passivating the {100} facets on very small Ag nanocubes. The mechanistic roles of these additives, along with the effects of their interactions with other species present in the reaction solution, were all systematically investigated. The concentration of SH^- was found to be a particularly effective parameter for tuning the edge length of the nanocubes. As a result of the understanding gained during the course of this study, Ag nanocubes with uniform edge lengths controllable in the range of 13−23 nm could be reliably produced. The nanocubes of 13.4 ± 0.4 nm in edge length constitute the smallest nanocrystals of this kind reported to date; they also possess sharper corners and edges relative to the limited examples of sub-20 nm Ag nanocubes reported in the literature. The availability of such small and sharp Ag nanocubes will open the door to an array of applications in plasmonics, catalysis, and biomedicine.

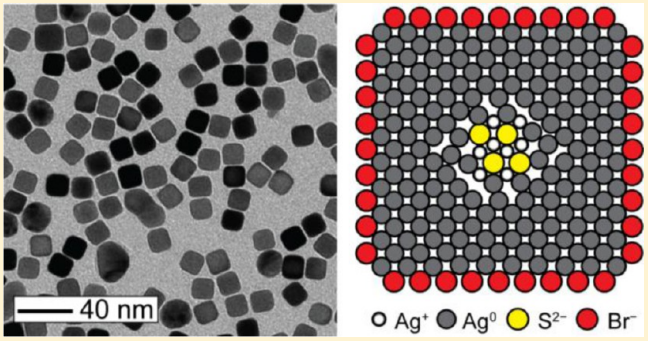

1. INTRODUCTION

For over a decade, intense research has been directed toward the development and refinement of protocols used for the synthesis of Ag nanocrystals with a broad range of well-controlled sizes and shapes.[1−11] The driving force stems from the potential utility of these nanocrystals in diverse applications, including photonics, electronics, catalysis, sensing, and medicine.[12−23] Among those Ag nanocrystals, nanocubes with sharp corners/edges and tunable edge lengths have garnered particular attention owning to their superb performance in applications involving localized surface plasmon resonance (LSPR)[24−28] and surface-enhanced Raman scattering (SERS).[29−31] When employed for the epoxidation of ethylene, Ag nanocubes have shown greater selectivity toward the production of ethylene oxide relative to both Ag nanospheres and irregular nanoparticles.[32,33] This result has been attributed to the fact that the surface of a Ag nanocube is near completely covered by {100} facets, whereas the surface of a nanosphere or irregular nanoparticle is covered by a mix of {100} and {111} facets. Moreover, Ag nanocubes have been used as sacrificial templates to generate hollow nanostructures (e.g., nanoboxes and nanocages) composed of Au, Pd, and Pt, which show promise as platform nanomaterials for drug delivery, imaging contrast enhancement, photothermal treatment, and plasmon-enhanced catalysis.[34,35]

The synthetic methods for the preparation of well-defined Ag nanocubes with narrow size distributions have been constantly refined over the past decade or so. In 2002, a one-pot protocol involving the use of ethylene glycol (EG) as both the solvent and reductant was reported.[4] In the following years, various refinements were introduced to optimize this synthesis. These include the introduction of HCl as an oxidative etchant,[36] the addition of sulfide (S^{2-}) and bisulfide (SH^-) ions to promote the formation of single-crystal seeds,[37] and the substitution of $AgNO_3$ by CF_3COOAg in an effort to achieve a higher degree of size control and better synthetic reproducibility.[38] More recently, EG was substituted by diethylene glycol (DEG), enabling the preparation of Ag nanocubes with edge lengths down to 18 nm.[39] Prior attempts to produce Ag nanocubes

Received: December 16, 2015
Published: February 15, 2016

DOI: 10.1021/jacs.5b13163
J. Am. Chem. Soc. 2016, 138, 3161−3167

below this size failed, primarily due to the high reduction rates present in the EG-based system, as well as ineffective surface capping by poly(vinylpyrrolidone) (PVP), a bulky, polymer-based capping agent for the Ag(100) surface. On the other hand, the Ag nanocubes produced using the DEG-based method displayed significant rounding at the corners and edges, particularly at sizes below 25 nm. Furthermore, the DEG-based synthesis was subsequently shown to be sensitive to variations in impurity levels between different batches of DEG, thereby lowering the overall reproducibility of that protocol.

Herein, we report an EG-based synthesis of Ag nanocubes having sharp corners and edges, together with edge lengths below 15 nm. The success of this synthesis relies on a tight control over the nucleation process through the addition of trace amounts of SH^- and the substitution of HCl by NaCl as the chloride source, as well as the use of Br^- as an effective capping agent for small-sized particles. The mechanistic roles of these additives on the nucleation and growth are systematically studied. The use of Br^- as a capping agent has been previously explored in the aqueous synthesis of Pd nanocubes/nanobars with sizes as small as 6 nm and seeded growth of Ag nanobars as small as 35 nm in a polyol-based system.[31,40−43] However, Br^- ions have not been exploited so far for the generation of Ag nanocubes with sharp corners/edges and small sizes down to 15 nm. To our knowledge, the Ag nanocubes presented herein are the smallest ever reported, while exhibiting a much higher degree of structural definition compared to previous reports. The potential applications of such small Ag nanocubes include their use as well-defined catalysts with higher surface-to-volume ratios. They can also serve as sacrificial templates for the production of small nanocages sought by both nanomedicine and catalysis.[35]

2. EXPERIMENTAL SECTION

Chemicals and Materials. Ethylene glycol (EG, ≥99.0%) was obtained from J. T. Baker (batch no. 0000034605). Silver trifluoroacetate (CF_3COOAg, ≥99.99%), sodium hydrosulfide hydrate ($NaHS{\cdot}1.5H_2O$), aqueous hydrochloric acid solution (HCl, 37%), poly(vinylpyrrolidone) (PVP, MW ≈ 55,000), sodium chloride (NaCl), sodium bromide (NaBr), and sodium sulfide nonahydrate ($Na_2S{\cdot}9H_2O$) were all obtained from Sigma-Aldrich. All chemicals were used as received. Deionized (DI) water with a resistivity of 18.2 MΩ·cm was used throughout the experiment. The synthesis of Ag nanocrystals was carried out in a 100 mL round-bottom flask (ACE Glass).

Synthesis of Ag Nanocubes. In a standard synthesis, 25 mL of EG were added into a flask and heated for 40 min under magnetic stirring in an oil bath set to 142 °C. A stable temperature of approximately 135 °C was measured for the reaction solution. Other reagents were separately dissolved in EG and sequentially introduced into the flask using a pipet. Specifically, 0.3 mL of NaSH solution (3.5 mM) was added first. After 4 min, 2.5 mL of NaCl solution (3 mM) was introduced, followed by 6.25 mL of PVP solution (20 mg/mL) 2 min later. After another 2 min, 2 mL of CF_3COOAg solution (282 mM) were introduced. Finally, 2.5 mL of NaBr solution (3 mM) were added after 5 min of delay. Note that the NaSH solution was prepared immediately before its injection. During the entire process, the flask was capped with a glass stopper except during the addition of reagents. The synthesis was quenched by immersing the flask in an ice−water bath. The solution was split into four portions, and 125 mg of PVP were dissolved in each fraction. This is necessary in order to prevent aggregation during the washing steps. The products were precipitated with acetone and collected by centrifugation at 6000 rpm for 10 min, followed by washing with DI water and centrifuging at 15 000 rpm for 15 min twice to remove the remaining precursor, EG, and excess PVP. If NaBr was used during the synthesis, the product solution was twice centrifuged at 4000 rpm for 30 min in order to separate the insoluble AgBr precipitate from the Ag nanocube solution.

Instrumentation. Transmission electron microscopy images were obtained using a Hitachi HT7700 microscope operated at 120 kV. UV−vis absorption spectra were recorded with a Lambda 750 spectrometer (PerkinElmer). An Eppendorf centrifuge (5430) was used for the collection and washing of all samples.

Nanocube Edge Length Analysis Methodology. The edge lengths of the produced Ag nanocubes were determined by analyzing TEM images with ImageJ software, with the averages and standard deviations calculated using functions built into Microsoft Excel. For each edge length analysis, 150 randomly selected (i.e., picked by the ImageJ software) nanocubes were used and the large, irregular nanoparticles were excluded from analysis.

3. RESULTS AND DISCUSSION

Synthesis of Small Ag Nanocubes. Figure 1 shows TEM images of the Ag nanocubes obtained by allowing different

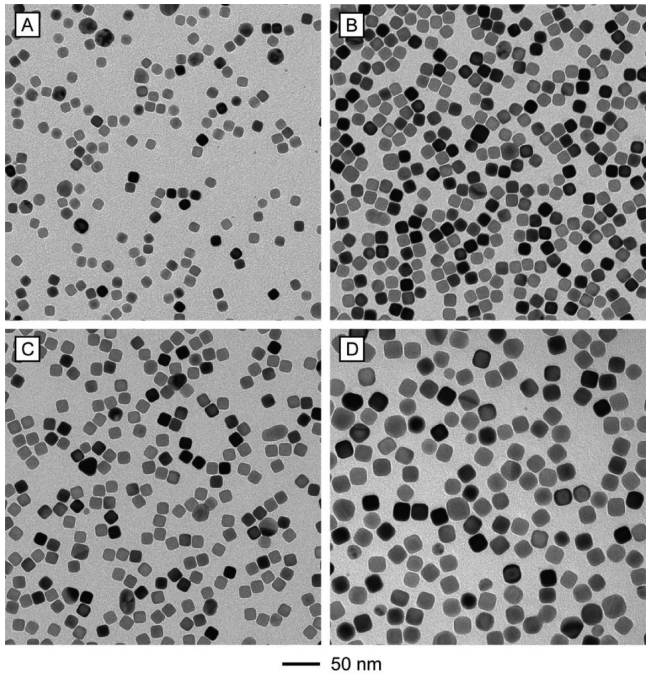

Figure 1. TEM images of Ag nanocubes synthesized with the use of different delay times before the introduction of Br^- ions: (A) 5, (B) 10, (C) 15, and (D) 25 min. The average edge lengths of the nanocubes were (A) 13.4 ± 0.4, (B) 15.3 ± 0.6, (C) 15.8 ± 0.4, and (D) 18.6 ± 0.7 nm.

periods of time to pass after the introduction of CF_3COOAg, but before the injection of NaBr solution. For the purposes of clarity, this period will be referred to as the delay time, while the time elapsed after the addition of NaBr will be referred to as the growth time. For the standard synthesis, the delay time and growth time were 5 and 15 min, respectively, and we obtained Ag nanocubes with an average edge length of 13.4 ± 0.4 nm, as shown in Figure 1A. A histogram showing the edge length distribution for this sample can be found in Figure S1. Extending the delay time to 10, 15, and 25 min, while keeping the growth time fixed, resulted in larger Ag nanocubes with average edge lengths of 15.3 ± 0.6, 15.8 ± 0.4, and 18.6 ± 0.7 nm, respectively, as shown in Figure 1B−D. At longer delay times, the edge length was capped at ∼23 nm, likely due to the depletion of all CF_3COOAg precursor. Further shortening the delay time did not generate Ag nanocubes with significantly

DOI: 10.1021/jacs.5b13163
J. Am. Chem. Soc. 2016, 138, 3161−3167

shorter edge lengths when compared with the standard synthesis. For instance, the use of a delay time of 1 min produced Ag nanocubes 12.7 ± 0.6 nm in edge length, as well as a large number of relatively large multiply twinned nanoparticles, as shown in Figure S2. Similarly, extending the growth time from 15 to 60 min only resulted in a marginal increase in edge length by 1.0 nm (Figure S3). The longer growth time did not compromise the corner and edge sharpness of the nanocubes. However, TEM images showed the formation of sub-5 nm particles in the solution when the growth time was increased, suggesting additional nucleation.

In order to study the evolution of corners and edges on small Ag nanocubes, we conducted syntheses at short growth times. Figure 2A–D show TEM images of the products obtained by varying the growth time from 0 to 15 min, in 5 min increments. Immediately after the addition of NaBr solution (Figure 2A), the product consisted of 11.7 ± 1.0 nm Ag spheres. In addition, a large number of sub-5 nm nanoparticles were observed. As the reaction continued, a fraction of cuboctahedra (i.e., nanocrystals with rounded corners and edges) would emerge, most noticeably at a growth time of 10 min (Figure 2C). Notably, the cuboctahedra then developed into nanocubes without any significant change to the edge length. Furthermore, the fraction of sub-5 nm particles decreased significantly, likely due to the Ostwald ripening effect. After 15 min of growth (Figure 2D), the product consisted of 13.1 ± 0.5 nm Ag nanocubes with sharp corners and edges, as well as a smaller fraction of irregular, multiply twinned particles of ∼20 nm in size. Overall, the purity of Ag nanocubes was over 90%. UV–vis spectra taken from the products after different growth times (Figure 2E) revealed little change to the optical features during the initial 10 min after the introduction of NaBr, with a single absorption peak positioned around 404 nm. However, after growth for 15 min, the absorption peak was red-shifted to 414 nm, and a shoulder peak appeared at 360 nm. This phenomenon coincided with the appearance of sharp structural features, such as corners and edges, for the majority of Ag nanocrystals present in the sample. A shoulder peak around 500 nm can be attributed to the presence of large irregular particles and/or aggregation of nanocrystals in the product, as has been noted in previous studies.[36−38] We further confirmed the good reproducibility of the standard procedure by comparing the UV–vis spectra recorded from three different batches of a synthesis of 13 nm Ag nanocubes. As shown in Figure S4, the UV–vis spectra overlap reasonably well, indicating good agreement in size and structural definition between the distinct batches.

We have also used TEM imaging to analyze the corner/edge sharpness of the final Ag nanocubes. First, a square outline was manually fitted over the 2-D TEM image of a Ag nanocube, simulating the perimeter of a completely sharp nanocube face. The area occupied by the truncated Ag nanocube in the TEM image was determined by manually subtracting the triangular areas of the missing corners from the area of the fitted square outline. An example is shown in Figure S5. We define the measure of nanocube sharpness as the ratio of the area of the Ag nanocube in the TEM image to the area of the fitted square outline, with the value of 1 denoting perfect sharpness. This can also be thought of as the extent of nanocube surface coverage by {100} facets. The final reported value is the simple average of measurements collected for 100 randomly selected nanocubes. For Ag nanocubes with edge lengths of 13.4 ± 0.4, 15.3 ± 0.6, and 18.6 ± 0.7 nm (Figure 1A–C), they were found to exhibit sharpness on the order of 0.96, 0.95, and 0.95, respectively. In comparison, the previously reported smallest 18 nm Ag nanocubes prepared using the DEG-based method only gave a sharpness measure of 0.90, thus highlighting the improvement of the new approach.[39]

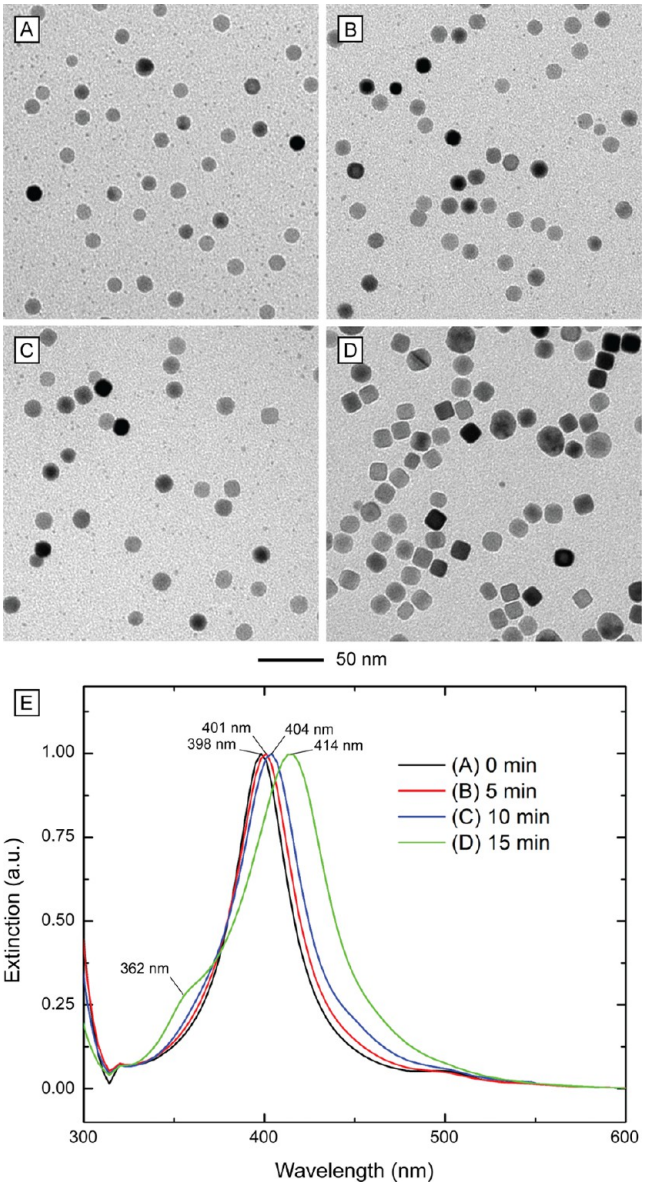

Figure 2. (A–D) TEM images of samples obtained using different growth times after the addition of Br^- ions: (A) 0, (B) 5, (C) 10, and (D) 15 min. (E) UV–vis spectra of the samples shown in (A–D). Note that the appearance of a shoulder peak at ∼360 nm, along with a 10 nm red-shift for the major peak, coincides with the emergence of sharp corners and edges on the nanocubes as revealed by TEM. The shoulder peak around 500 nm can be attributed to the presence of large irregular particles and/or aggregation of nanocrystals in the product.

Effects of SH^- on Ag Nucleation. In principle, there exists two different pathways for Ag atoms to nucleate: homogeneous and heterogeneous. Homogeneous nucleation necessitates the presence of a supersaturated concentration of free Ag atoms, which can be obtained through steady reduction of a salt precursor. Once supersaturation has been achieved, the free Ag atoms coalesce into small clusters, which then serve as nuclei for further growth. The rapid growth quickly consumes the

DOI: 10.1021/jacs.5b13163
J. Am. Chem. Soc. 2016, 138, 3161−3167

available Ag atoms, thereby bringing down the concentration of Ag atoms below the supersaturation threshold and ultimately quenching the nucleation process. In contrast, heterogeneous nucleation is characterized by the deposition of Ag atoms onto locally available surfaces, without requiring a supersaturated environment. This is due to an intrinsically lower free energy barrier for heterogeneous nucleation as compared to homogeneous nucleation. As a consequence of this imbalance, heterogeneous nucleation occurs much more rapidly when compared with its counterpart. Based on this information, it should be possible to create a large number of Ag nanocrystals by purposely introducing cluster-sized, insoluble impurities, analogous to those produced by homogeneous nucleation, into the reaction solution to serve as sites for rapid heterogeneous nucleation and growth. The number of these nucleation sites will determine the size of the final Ag nanocrystals, since the fixed number of Ag atoms available from the precursors are supposed to be evenly divided among the nuclei during growth. Thus, a larger number of nuclei will produce smaller Ag nanocrystals, and vice versa.

The bisulfide-assisted polyol synthesis of monodisperse Ag nanocubes is an example of this approach, as previously reported by our group.[37,38] In those reports, we posited that bisulfide (SH^-) and Ag^+ ions quickly react to produce highly insoluble Ag_2S clusters ($K_{sp} = 10^{-52}$), which then serve as sites for the rapid heterogeneous nucleation of Ag atoms and subsequent formation of single-crystal nanocubes. The produced Ag_2S cluster is too small for the lattice mismatch between Ag_2S (monoclinic) and Ag (face-centered cubic) to impact the crystal structure of the nanocrystal beyond the few initially deposited layers of Ag. As a result, uniform Ag nanocubes with an edge length as short as 30 nm could be prepared in an EG-based system containing a trace amount of SH^- (27 μM). Figure 3 shows a mechanistic illustration of this

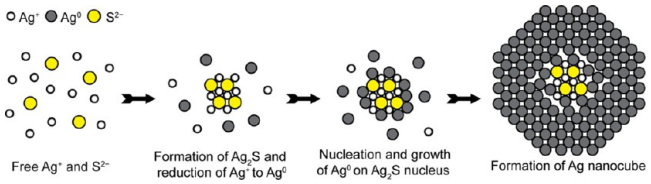

Figure 3. Schematic illustration showing the formation of Ag nanocubes through heterogeneous nucleation and growth on Ag_2S-based nuclei, enabled by the addition of a trace amount of SH^-. The Ag_2S nuclei are immediately formed upon the introduction of a Ag^+ precursor, followed by the deposition of Ag^0 atoms to yield Ag nanocubes.

approach. A subsequently developed protocol reduced the edge length of the nanocubes down to 18 nm by replacing EG with DEG.[39] In both cases, an HCl solution was added as a source of Cl^-, necessary to modulate the reaction kinetics and provide a source of mild oxidative etching. Specifically, the addition of Cl^- creates AgCl ($K_{sp} = 10^{-10}$) in solution, which dissolves over time, unlike Ag_2S. This regulates the amount of Ag^+ available for reduction in the initial stages of the synthesis, thereby allowing for control over reaction kinetics. Oxidative etching can be understood as a redox reaction between Ag atoms and dissolved O_2 gas, with Cl^- acting as a charge carrier.[44] Figure 4A and B show the products of a standard synthesis taken at 20 and 30 min after the introduction of a Ag precursor, respectively, with HCl serving as a source of chloride and

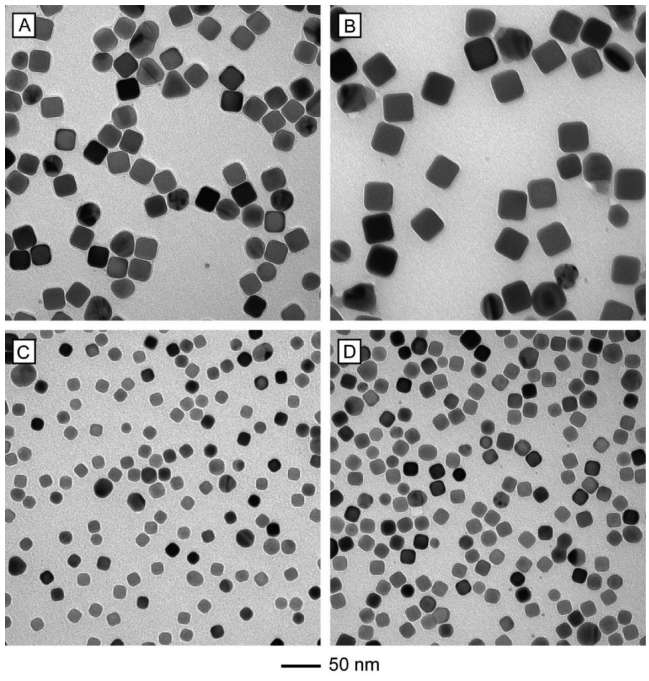

Figure 4. TEM images of reaction products obtained in the presence of (A, B) HCl and (C, D) NaCl, together with growth times of (A, C) 15 min and (B, D) 25 min, respectively. All other conditions were kept the same as in the standard synthesis.

without adding any NaBr. The average edge lengths were measured to be 25.4 ± 1.3 and 35.0 ± 1.0 nm at 20 and 30 min post-Ag-precursor addition, respectively. This corresponds to a 161% change in volume for the Ag nanocubes over a growth time of 10 min, demonstrating very rapid growth, and suggesting that a large number of Ag atoms remained in the reaction solution after nucleation. At first glance, such quick growth appears to be at odds with the idea of a large number of nuclei present in the system, as we expect the available Ag precursors to be rapidly drained via heterogeneous nucleation in the early stage of a synthesis.

A closer look at the interactions between the reactants, and their influence on the mechanism responsible for the formation of the initial Ag_2S clusters, may provide the answer. The molar ratio of dissociated H^+ to SH^- present in the final reaction solution was 8.3:1, with HCl being introduced into the system immediately after the introduction of SH^- and before the injection of the Ag precursor. This consecutive addition, coupled with an excess of H^+, likely results in a rapid recombination reaction between H^+ and SH^- ions, thereby irreversibly producing H_2S and consuming the free SH^- entirely. From previous measurements, the solubility of H_2S in EG at 125 °C can be estimated to be 1.87 g per kg, which is sufficient to dissolve all the newly produced H_2S gas, even assuming full conversion of SH^- to H_2S.[45,46] The removal of free SH^- ions essentially blocks the initial formation of Ag_2S clusters. As a result, the initial nucleation of Ag atoms has to proceed through a homogeneous route, with the newly formed Ag^0 atoms being likely oxidized back to Ag^+ via a combination of the dissolved H_2S and O_2 to generate insoluble Ag_2S. However, due to the higher energies needed to drive homogeneous nucleation relative to heterogeneous nucleation, this indirect process produces far fewer Ag_2S clusters when compared with the proposed direct formation of Ag_2S from Ag^+

DOI: 10.1021/jacs.5b13163
J. Am. Chem. Soc. 2016, 138, 3161−3167

and SH^- ions. In turn, this allows for a high concentration of Ag precursor to remain in the reaction solution, resulting in rapid growth for the nanocrystals and the formation of large Ag nanocubes, as shown in Figure 4A and B. We have attempted to quantify the amount of S present in the Ag nanocubes with both inductively coupled plasma mass spectrometry (ICP-MS) and energy-dispersive X-ray spectroscopy (EDX) elemental mapping. In the case of the former, the S signal was interfered with by signals from Ar and O_2, both of which are present in large quantities during a measurement under ambient conditions, thus precluding accurate analysis. In the case of the latter, the collected S signal was below the noise level of the EDX measurement, due to a very small S/Ag elemental ratio.

By substituting HCl with NaCl, the source of protons would be removed from the system, thus restoring the original Ag_2S cluster formation mechanism. Figure 4C and D show the product of a standard synthesis collected at 20 and 30 min after the addition of the Ag precursor, respectively, with NaCl substituting HCl as the source of Cl^- while no NaBr was added. The average edge length was measured to be 15.2 ± 0.6 and 18.1 ± 0.5 nm at 20 and 30 min post-Ag-precursor addition, respectively, corresponding to a 69% increase in volume for the Ag nanocubes over 10 min. This value is less than half of the rate of growth seen in the HCl-mediated synthesis. The significantly slower growth rate suggests the formation of a larger number of Ag_2S clusters during the nucleation stage as compared to the HCl system. The result is the rapid consumption of available Ag precursor, slowing down the growth and thus generating smaller Ag nanocubes.

Previous work has shown that EG oxidizes into glycolaldehyde in the presence of dissolved O_2 and at temperatures above 100 °C.[47,48] The glycolaldehyde acts as the primary reducing agent, being oxidized further into a carboxylic acid and producing protons in the process. Additional H^+, introduced by the HCl, can slow the oxidation of glycolaldehyde, thus inhibiting the reduction process and slowing the nanocube nucleation and growth. The removal of these protons in the case of the NaCl-based synthesis would have the opposite effect. In either case, however, the trace amounts of H^+ (~191 μM) introduced with the HCl should have no significant impact on pH and reduction kinetics. Furthermore, previous attempts to increase the reduction kinetics by increasing temperature have not produced smaller Ag nanocubes.[38] Therefore, the decrease in size for the nanocubes can be largely attributed to the increased number of heterogeneous nucleation sites in the reaction system.

To further study the influence of SH^- on the size of Ag nanocubes, we conducted syntheses at various concentrations of NaSH without the addition of NaBr. Figure 5 shows TEM images of the products obtained from syntheses that were undersupplied (Figure 5A) and oversupplied with SH^- (Figure 5B) compared to the standard SH^- concentration. Specifically, the nanoparticles in Figure 5A were prepared using a 0.58 mM NaSH solution, which corresponds to one-sixth the standard concentration, and those in Figure 5B were obtained with a 7 mM NaSH solution, corresponding to twice the standard concentration. In the former case, Ag nanocubes with an average edge length of ~23 nm were obtained, along with a large fraction of multiply twinned nanoparticles. The latter produced a majority fraction of ~7 nm spherical particles and a minor fraction of ~30 nm cuboctahedra, shown in the inset of Figure 5B. The cuboctahedra in the minority fraction formed a coffee ring pattern on the TEM grid, thereby effectively isolating them from the bulk of the imaged sample. Notably, the larger cuboctahedra were likely produced in the first moments after the mixing of the Ag precursor, with the slow subsequent growth failing to narrow the overall size distribution of the product. These results are consistent with our established hypothesis: a lower concentration of SH^- resulted in fewer Ag_2S clusters for heterogeneous nucleation and thus larger Ag nanocubes, while a higher-than-standard concentration of SH^- produced too many Ag_2S nuclei, which consumed the Ag precursor too quickly and resulted in smaller cuboctahedra. These cuboctahedra likely failed to develop into nanocubes due to the lack of sufficient Ag for growth, as well as the inability of the long-chain PVP macromolecules to stabilize the {100} facets at such a small size.

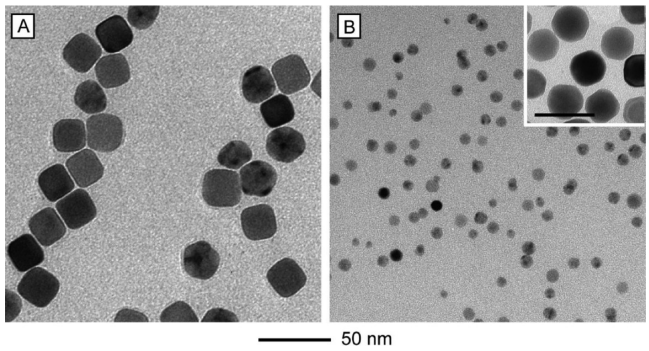

Figure 5. TEM images of reaction products obtained with the use of NaSH solutions at different concentrations: (A) 0.6 mM and (B) 6 mM, respectively. All other conditions were kept the same as in the standard synthesis. The inset in (B) shows the minority product fraction, consisting of ~30 nm Ag cuboctahedra. The cuboctahedra in the minority fraction formed a coffee ring pattern on the TEM grid, thereby isolating them from the bulk of the imaged sample. The scale bar in the inset corresponds to 50 nm.

Finally, in order to rule out the possible influence of the sulfide source, we performed a set of control experiments, in which we substituted $NaHS{\cdot}1.5H_2O$ in the standard procedure with the same molar concentration of $Na_2S{\cdot}9H_2O$. Figure S6 shows TEM images of Ag nanocubes with average edge lengths of 12.7 ± 0.5 and 18.1 ± 0.7 nm produced with the addition of Na_2S by varying the delay time from 5 to 25 min, respectively. These results suggest that good quality nanocubes could be produced irrespective of whether S^{2-} or SH^- was introduced into the reaction system, which is consistent with previous findings.[37] However, it should be pointed out that $NaHS{\cdot}1.5H_2O$ is less hygroscopic and therefore much easier to accurately weight out in small quantities during preparation, allowing for greater synthetic reproducibility.

Influence of Br^- Ions. The impact of introducing a trace amount of Br^- into the reaction system is twofold. First, the bromide ions can act as a selective capping agent toward the Ag{100} facets, thereby promoting the formation of nanocrystals with a cubic shape. This behavior has been well studied with regard to the one-pot synthesis of Pd nanocubes/nanobars and seeded growth of Ag nanospheres into nanobars.[31,43] In contrast to the latter, the product of the synthesis presented herein consists largely of nanocubes, with some nanobars emerging at extended growth times (Figure S3C and D). Second, the Br^- ions quickly bind with the remaining Ag^+ ions in the reaction solution, forming largely insoluble AgBr (K_{sp} = 10^{-14}) and effectively abstracting nearly all available Ag precursor from the reaction. The addition of NaBr after a

DOI: 10.1021/jacs.5b13163
J. Am. Chem. Soc. 2016, 138, 3161−3167

certain delay time effectively delineates the point between fast and slow reduction kinetics, with the formation of single-crystal seeds occurring during the former and the growth of nanocubes proceeding during the latter. The AgBr precipitate can be easily collected and removed through centrifugation after the reaction has been completed. The remaining Ag atoms grow on the {111} facets of the nucleated Ag cuboctahedra, as directed by the capping of Br^- toward the Ag(100) surface, to generate the corners on the final nanocubes. As discussed previously, all subsequent growth for the nanocubes was extremely slow, with Ag atoms involved in the growth likely released through the dissolution of initially formed AgCl precipitates and Cl^--mediated oxidative etching. Additionally, the lack of a significant population of Ag nanobars, even at prolonged growth times, is likely due to the rapid rate of diffusion for Ag atoms on the surface, significantly exceeding the rate of growth.[49] As a result, there is a more or less even distribution of Ag atoms across the entire surface of a growing nanocrystal, thus producing nanocubes rather than nanobars as the major product fraction.

In order to explore the influence of Br^- concentration on the morphology of final products, we conducted a set of experiments with different amounts of Br^- being introduced. Figure 6 shows the products obtained using the standard

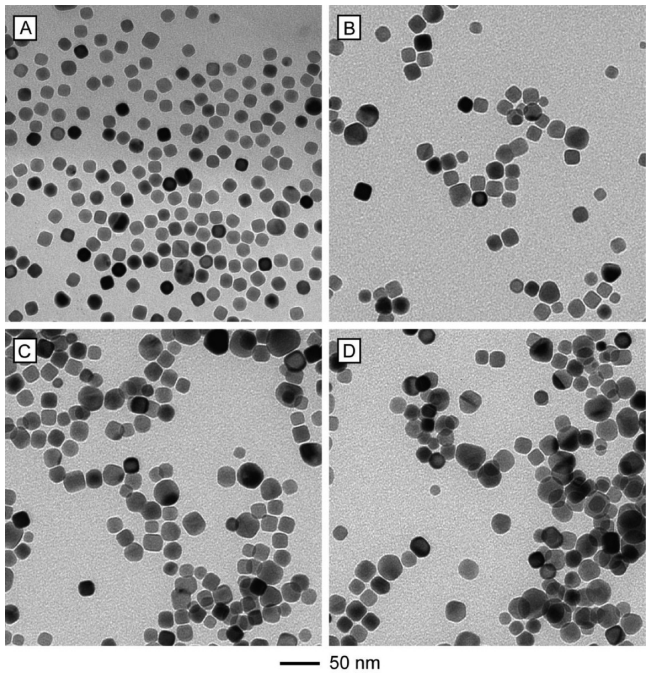

Figure 6. TEM images of reaction products obtained with the use of NaBr solutions at different concentrations: (A) 0, (B) 15, (C) 30, and (D) 90 mM. The growth time was 15 min, while all other parameters were kept the same as in the standard synthesis.

procedure, except for the variation in NaBr concentration. When no NaBr was added, the synthesis yielded a mixture of Ag cuboctahedra and nanocubes, with an average edge length of 15.3 ± 0.7 nm, as shown in Figure 6A. When the concentration of NaBr was increased, a decrease in both nanocube uniformity and product purity was observed (Figure 6B–D). The polydispersity of size, in the range of 13–23 nm, as well as the emergence of a significant fraction of large, rounded nanoparticles, suggests that higher concentrations of NaBr further slow down the reaction kinetics in the growth stage of the synthesis. While the exact mechanism is still unclear, it is possible that the excessive Br^- ions could abstract the Ag^+ ions produced by secondary pathways, such as oxidative etching and Oswald ripening, effectively starving the system of growth material and thereby leading to the aberrant growth regimes seen in Figure 6C and D.

4. CONCLUSION

In conclusion, we have successfully developed a polyol-based method for generating well-defined Ag nanocubes with edge lengths below 15 nm. The success of this method relies on a combination of the effective capping of small Ag{100} facets by Br^- ions and control over the number of nuclei initially formed in the reaction system. The latter was enabled by a new understanding of the mechanistic effects of SH^- additives, achieved over the course of this work. The substitution of HCl by NaCl as the chloride source improved upon previous synthetic methods, greatly enhancing the effectiveness of the SH^- additive in controlling the nucleation of Ag atoms. As a result, the variation of SH^- concentration was shown to be an effective means for controlling the edge length of Ag nanocubes. The Br^- ions acted as both a capping agent toward the Ag(100) surface and a kinetic regulator by limiting the number of free Ag^0 atoms present in the reaction solution. The resultant Ag nanocubes are both smaller and sharper at corners/edges when compared with those reported in previous work. The edge length of the nanocubes could be readily varied from 13 to 23 nm by quenching the synthesis after different periods of growth. The nanocube yield was estimated to be ~90%, and subsequent experiments have shown this approach to be both highly reproducible and readily scalable.

■ ASSOCIATED CONTENT

Supporting Information

The Supporting Information is available free of charge on the ACS Publications website at DOI: 10.1021/jacs.5b13163.

Size distribution of nanocube products; TEM images of products obtained at a very short delay time; TEM images of products obtained at prolonged growth times; UV–Vis spectra of different product batches illustrating reproducibility; illustration of TEM analysis conducted to determine the corner/edge sharpness of the Ag nanocubes; products obtained after substituting the sulfide source (PDF)

■ AUTHOR INFORMATION

Corresponding Author

*younan.xia@bme.gatech.edu

Notes

The authors declare no competing financial interest.

■ ACKNOWLEDGMENTS

This work was supported in part by research grants from the NSF (DMR 1506018) and the NIH (R01 CA 138527). A.R. was supported by a Graduate Research Fellowship from the NSF.

■ REFERENCES

(1) Rycenga, M.; Cobley, C. M.; Zeng, J.; Li, W.; Moran, C. H.; Zhang, Q.; Qin, D.; Xia, Y. *Chem. Rev.* **2011**, *111*, 3669–3712.

DOI: 10.1021/jacs.5b13163
J. Am. Chem. Soc. 2016, 138, 3161–3167

(2) Jin, R.; Cao, Y.; Mirkin, C. A.; Kelly, K. L.; Schatz, G. C.; Zheng, J. G. *Science* **2001**, *294*, 1901−1903.
(3) Jana, N. R.; Gearheart, L.; Murphy, C. J. *Chem. Commun.* **2001**, 617−618.
(4) Sun, Y.; Xia, Y. *Science* **2002**, *298*, 2176−2179.
(5) Tao, A. R.; Sinsermsuksakul, P.; Yang, P. *Angew. Chem., Int. Ed.* **2006**, *45*, 4597−4601.
(6) Zhang, J.; Li, S.; Wu, J.; Schatz, G. C.; Mirkin, C. A. *Angew. Chem., Int. Ed.* **2009**, *48*, 7787−7791.
(7) Murshid, N.; Kitaev, V. *Chem. Commun.* **2014**, *50*, 1247−1249.
(8) Keunen, R.; Cathcart, N.; Kitaev, V. *Nanoscale* **2014**, *6*, 8045−8051.
(9) Xia, X.; Zeng, J.; Zhang, Q.; Moran, C. H.; Xia, Y. *J. Phys. Chem. C* **2012**, *116*, 21647−21656.
(10) Langille, M. R.; Personick, M. L.; Mirkin, C. A. *Angew. Chem., Int. Ed.* **2013**, *52*, 2−33.
(11) Wiley, B. J.; Im, S. H.; Li, Z.-Y.; McLellan, J.; Siekkinen, A.; Xia, Y. *J. Phys. Chem. B* **2006**, *110*, 15666−15675.
(12) Lu, G.; De Keersmaecker, H.; Su, L.; Kenens, B.; Rocha, S.; Fron, E.; Chen, C.; Van Dorpe, P.; Mizuno, H.; Hofkens, J.; Hutchison, J. A.; Uji-I, H. *Adv. Mater.* **2014**, *26*, 5124−5128.
(13) Zeng, S.; Baillargeat, D.; Ho, H.-P.; Yong, K.-T. *Chem. Soc. Rev.* **2014**, *43*, 3426−3452.
(14) Xue, B.; Wang, D.; Zuo, J.; Kong, X.; Zhang, Y.; Liu, X.; Tu, L.; Chang, Y.; Li, C.; Wu, F.; Zeng, Q.; Zhao, H.; Zhao, H.; Zhang, H. *Nanoscale* **2015**, *7*, 8048−8057.
(15) Lee, S.; Shin, S.; Lee, S.; Seo, J.; Lee, J.; Son, S.; Cho, H. J.; Algadi, H.; Al-Sayari, S.; Kim, D. E.; Lee, T. *Adv. Funct. Mater.* **2015**, *25*, 3114−3121.
(16) Mayousse, C.; Celle, C.; Fraczkiewicz, A.; Simonato, J.-P. *Nanoscale* **2015**, *7*, 2107−2115.
(17) Kawawaki, T.; Wang, H.; Kubo, T.; Saito, K.; Nakazaki, J.; Segawa, H.; Tatsuma, T. *ACS Nano* **2015**, *9*, 4165−4172.
(18) Linic, S.; Christopher, P.; Xin, H.; Marimuthu, A. *Acc. Chem. Res.* **2013**, *46*, 1890−1899.
(19) Stark, W. J.; Stoessel, P. R.; Wohlleben, W.; Hafner, A. *Chem. Soc. Rev.* **2015**, *44*, 5793−5805.
(20) Verano-Braga, T.; Miethling-Graff, R.; Wojdyla, K.; Rogowska-Wrzesinska, A.; Brewer, J. R.; Erdmann, H.; Kjeldsen, F. *ACS Nano* **2014**, *8*, 2161−2175.
(21) Mu, Q.; Jiang, G.; Chen, L.; Zhou, H.; Fourches, D.; Tropsha, A.; Yan, B. *Chem. Rev.* **2014**, *114*, 7740−7781.
(22) Liang, R.; Wei, M.; Evans, G. E.; Duan, X. *Chem. Commun.* **2014**, *50*, 14071−14081.
(23) Le Ouay, B.; Stellacci, F. *Nano Today* **2015**, *10*, 339−354.
(24) Sherry, L. J.; Chang, S.-H.; Schatz, G. C.; Van Duyne, R. P. *Nano Lett.* **2005**, *5*, 2034−2038.
(25) Konig, T. A. F.; Ledin, P. A.; Kerszulis, J.; Mahmoud, M. A.; El-Sayed, M. A.; Reynolds, J. R.; Tsukruk, V. V. *ACS Nano* **2014**, *8*, 6182−6192.
(26) Klimov, V.; Guo, G.-Y.; Pikhota, M. J. *J. Phys. Chem. C* **2014**, *118*, 13052−13058.
(27) Bordley, J. A.; Hooshmand, N.; El-Sayed, M. A. *Nano Lett.* **2015**, *15*, 3391−3397.
(28) Li, G.; Cherqui, C.; Bigelow, N. W.; Duscher, G.; Straney, P. J.; Millstone, J. E.; Masiello, D. J.; Camden, J. P. *Nano Lett.* **2015**, *15*, 3465−3471.
(29) Yang, Y.; Matsubara, S.; Xiong, L.; Hayakawa, T.; Nogami, M. *J. Phys. Chem. C* **2007**, *111*, 9095−9104.
(30) Prezgot, D.; Ianoul, A. *J. Phys. Chem. C* **2015**, *119*, 3293−3301.
(31) Zhang, Q.; Moran, C. H.; Xia, X.; Rycenga, M.; Li, N.; Xia, Y. *Langmuir* **2012**, *28*, 9047−9054.
(32) Christopher, P.; Linic, S. *J. Am. Chem. Soc.* **2008**, *130*, 11264−11265.
(33) Christopher, P.; Linic, S. *ChemCatChem* **2010**, *2*, 78−83.
(34) Skrabalak, S. E.; Chen, J.; Sun, Y.; Lu, X.; Au, L.; Cobley, C. M.; Xia, Y. *Acc. Chem. Res.* **2008**, *41*, 1587−1595.
(35) Xia, X.; Wang, Y.; Ruditskiy, A.; Xia, Y. *Adv. Mater.* **2013**, *25*, 6313−6333.
(36) Im, S. H.; Lee, Y. T.; Wiley, B.; Xia, Y. *Angew. Chem., Int. Ed.* **2005**, *44*, 2154−2157.
(37) Siekkinen, A. R.; McLellan, J. M.; Chen, J.; Xia, Y. *Chem. Phys. Lett.* **2006**, *432*, 491−496.
(38) Zhang, Q.; Li, W.; Wen, L.-P.; Chen, J.; Xia, Y. *Chem. - Eur. J.* **2010**, *16*, 10234−10239.
(39) Wang, Y.; Zheng, Y.; Huang, C. Z.; Xia, Y. *J. Am. Chem. Soc.* **2013**, *135*, 1941−1951.
(40) Wiley, B. J.; Chen, Y.; McLellan, J. M.; Xiong, Y.; Li, Z.-Y.; Ginger, D.; Xia, Y. *Nano Lett.* **2007**, *7*, 1032−1036.
(41) Wiley, B. J.; Xiong, Y.; Li, Z.-Y.; Yin, Y.; Xia, Y. *Nano Lett.* **2006**, *6*, 765−768.
(42) Jin, M.; Liu, H.; Zhang, H.; Xie, Z.; Liu, J.; Xia, Y. *Nano Res.* **2011**, *4*, 83−91.
(43) Peng, H.-C.; Xie, S.; Park, J.; Xia, X.; Xia, Y. *J. Am. Chem. Soc.* **2013**, *135*, 3780−3783.
(44) Zheng, Y.; Zeng, J.; Ruditskiy, A.; Liu, M.; Xia, Y. *Chem. Mater.* **2014**, *26*, 22−33.
(45) Jou, F.-Y.; Deshmukh, R. D.; Otto, F. D.; Mather, A. E. *Chem. Eng. Commun.* **1990**, *87*, 223−231.
(46) Short, I.; Sahgal, A.; Hayduk, W. *J. Chem. Eng. Data* **1983**, *28*, 63−66.
(47) Skrabalak, S. E.; Wiley, B. J.; Kim, M.; Formo, E. V.; Xia, Y. *Nano Lett.* **2008**, *8*, 2077−2081.
(48) Zhang, Q.; Cobley, C.; Au, L.; McKiernan, M.; Schwartz, A.; Wen, L.-P.; Chen, J.; Xia, Y. *ACS Appl. Mater. Interfaces* **2009**, *1*, 2044−2048.
(49) Xia, X.; Xie, S.; Liu, M.; Peng, H.-C.; Lu, N.; Wang, J.; Kim, M. J.; Xia, Y. *Proc. Natl. Acad. Sci. U. S. A.* **2013**, *110*, 6669−6673.

DOI: 10.1021/jacs.5b13163
J. Am. Chem. Soc. 2016, 138, 3161−3167